Precise Photoexcitation Measurement of Tan's Contact in the Entire BCS-BEC Crossover

Manuel Jäger and Johannes Hecker Denschlag

Institut für Quantenmaterie and Center for Integrated Quantum Science and Technology (IQST), Universität Ulm,
Albert-Einstein-Allee 45, 89081 Ulm, Germany

We study two-body correlations in a spin-balanced ultracold harmonically trapped Fermi gas of ^{6}Li atoms in the crossover from the Bardeen-Cooper-Schrieffer (BCS) to the Bose-Einstein-Condensate (BEC) regime. For this, we precisely measure Tan's contact using a novel method based on photoexcitation of atomic pairs, which was recently proposed by Wang *et al.* [Photoexcitation measurement of Tan's contact for a strongly interacting Fermi gas, Phys. Rev. A **104**, 063309 (2021).]. We map out the contact in the entire phase diagram of the BCS-BEC crossover for various temperatures and interaction strengths, probing regions in phase space that have not been investigated yet. Our measurements reach an uncertainty of $\approx 2\%$ at the lowest temperatures and thus represent a precise quantitative benchmark. By comparison to our data, we localize the regions in phase space where theoretical predictions and interpolations give valid results. In regions where the contact is already well known we find excellent agreement with our measurements. Thus, our results demonstrate that photoinduced loss is a precise probe to measure quantum correlations in a strongly interacting Fermi gas.

A Fermi gas of ultracold atoms with tunable interactions is an excellent platform for studying pair correlations and superfluidity. The interactions can be controlled, e.g., via a magnetically tunable Feshbach resonance where the scattering state of two atoms is coupled to a weakly bound molecular state of a closed channel at close range. This allows for investigating the crossover from the BCS to the BEC regime, where the system fundamentally changes its physical character. In the weakly interacting BCS regime, weakly bound Cooper pairs form on the surface of the atomic Fermi sea with its strong interparticle correlations, while in the BEC regime fermionic atoms combine to form tightly bound bosonic molecules with small correlations between them. Tan's contact, first introduced by Tan in 2008 [1–3], is a measure for short-range two-body correlations and quantifies the likelihood of finding two interacting fermions at very small distance. From a thermodynamical point of view the total contact $\mathcal{I}$ is an extensive quantity, linearly scaling with the system size. It appears in a number of important thermodynamic relations for a strongly interacting Fermi gas.

The contact and several of its thermodynamic relations have been investigated experimentally in various approaches, including radio-frequency (rf) spectroscopy [4–6], mapping of the momentum distribution [4,7], Bragg spectroscopy [8], and collisional decay [9,10]. In recent years, contact measurements reached uncertainties as low as 2% [6–8]. So far, however, contact investigations were only carried out in particular areas of phase space, i.e., close to unitarity and at the lowest temperatures. A precise and comprehensive study across the entire phase diagram of the BCS-BEC crossover, providing a full picture of the contact, has been missing.

Tan's contact is expected to change smoothly from the BCS to the BEC limit, but precise calculations of the contact are still challenging especially in the regime of strong, near resonant interactions between the particles. Therefore, precise measurements in this area will result in an important step forward towards a complete understanding of the crossover physics.

Here, we provide a high precision measurement of Tan's contact across the full phase diagram of the BCS-BEC crossover for temperatures up to two times the Fermi temperature T_F. Because of a careful calibration the data reach a combined statistical and systematic uncertainty of $\approx 2\%$ for the lowest temperatures ($T \approx 0$), and up to 10% for $T/T_F \approx 1.5$. Therefore, they represent a quantitative benchmark to test theoretical model predictions. For the contact measurements, we demonstrate yet another method, which is based on laser-induced loss in the atomic gas, as outlined in [11]. Atom pairs at close range are photoexcited to a short-lived excited molecular bound state, producing an atom loss rate which is proportional to Tan's contact. In our specific system, photoexcitation occurs via a coherent admixture of a closed-channel molecular bound state to the pair wave function. This closed-channel bound state is also responsible for the Feshbach resonance. Measurements of the closed-channel fraction have been previously measured in the group of Hulet [12] and in the group of Pan [13] and they are closely related to the method reported here. The measured closed-channel fraction in [13] indicated a deviation by a factor of 3 from the well-understood theoretical predictions on the BCS side. This deviation does not occur in our measurements.

263401-1

Photoinduced two-body loss.—As pointed out in [14,15] there is a very general and fundamental link between the total contact $\mathcal{I}$ and the two-body loss rate of a two-component Fermi gas

$$-\frac{dN}{dt} = \frac{-\hbar \text{Im}[a]}{2\pi m |a|^2} \mathcal{I}, \qquad (1)$$

where N is the total atom number, m is the atomic mass, and a is the scattering length. If a has a finite imaginary part, loss due to a two-body process is present. Thus, the total contact of the spin-balanced Fermi gas can be simply deduced from the induced two-body loss rate. This is quite intuitive as two-body loss goes naturally along with two atoms being at close range. Equation (1) holds for collisional losses in s-wave collisions. For losses in p-wave collisions, a similar relation was recently found [10,16].

We now consider the special situation where an atomic s-wave collision takes place in the vicinity of a single, magnetically tunable, intrinsically lossless Feshbach resonance. Furthermore, two-body loss is induced via resonant photoexcitation of an atom pair at close range to an electronically excited, short-lived molecular state with a lifetime $1/\gamma$. For photoexcitation, the bare, closed-channel bound state of the Feshbach resonance is coupled to the excited molecular state with Rabi frequency Ω. For this system, Ref. [11] has calculated the complex scattering length a and Eq. (1) becomes

$$-\frac{dN}{dt} = \frac{\hbar \mathcal{I}}{2\pi m a_{bg}} \frac{\Omega^2/(2\gamma W)}{[1 - a_{bg}/a_s]^{-2} + [\Omega^2/(2\gamma W)]^2}. \qquad (2)$$

Here, a_s denotes the real-valued scattering length without the photoexcitation coupling, a_{bg} is the corresponding background scattering length and W the width of the Feshbach resonance. For all practical purposes, the term $[\Omega^2/(2\gamma W)]^2$ in the denominator can be neglected in our experiments.

Experiment.—For our measurements we use an ultracold Fermi gas of ^{6}Li atoms in the two lowest hyperfine states $|F = 1/2, m_F = 1/2\rangle$ and $|F = 1/2, m_F = -1/2\rangle$ with $N/2$ atoms per spin state. The atoms are trapped in a 3D harmonic trap which consists of a combination of an optical dipole trap and a magnetic trap. The atom cloud is cigar shaped, corresponding to the trapping frequencies $\omega_{ax} = 2\pi \times 21$ Hz in axial and $\omega_r = 2\pi \times 150\text{–}2000$ Hz in radial direction, respectively. Using forced evaporative cooling at a magnetic field of around 790 G we set a precise atomic temperature in the range of 0.04–2 T_F for clouds with atom numbers between 5×10^5 and 2×10^6. For a harmonically trapped gas, the Fermi temperature is given by $T_F = E_F/k_B = \hbar(\omega_{ax}\omega_r^2 3N)^{1/3}/k_B$, where E_F is the Fermi energy and k_B is the Boltzmann constant. By tuning the magnetic field B, we control the particle interaction with the help of the broad s-wave Feshbach resonance at 832.18(8) G [17], which allows for entering both the BCS ($a_s < 0$) and BEC regimes ($a_s > 0$) of the crossover. For this resonance the width is $W = -2\mu_B \times 262.3(3)$ G $= -2\pi\hbar \times 734(1)$ MHz, and $a_{bg} = -1582(1)a_0$ [17] where a_0 is the Bohr radius.

To optically induce two-body loss, we excite atom pairs, bound or unbound, to a deeply bound molecular level with vibrational quantum number $v' = 68$ in the electronically excited state $A^1\Sigma_u^+$ with a linewidth of $\gamma = 2\pi \times 12(1)$ MHz, as measured in our experiment [18]. For this, we make use of the fact that the initial atom pair wave function has an admixture from the (bare) molecular state $X^1\Sigma_g^+(v = 38)$, from which the state $A^1\Sigma_u^+(v' = 68)$ can be reached via an electric dipole transition [12]. The photoexcitation scheme is shown in Fig. 5 of [22]. To drive the transition we employ a 673 nm laser beam with an intensity of a few μW/cm^2 (where $\Omega \lesssim 2\pi \times 1$ MHz). At each magnetic field, the laser is tuned to be resonant on the photoexcitation transition. The photoexcitation leads to a decay of the total atom number N within a few hundred milliseconds. This slow decay ensures that the system stays in thermal equilibrium during the exposure. This is in contrast to previous experiments of ours where we used fast loss to measure the pair fraction in the Fermi gas, see [23].

We use high-field absorption imaging to measure the number of the remaining atoms, bound or unbound, as described in [23,24]. Pairs that had been previously photoexcited to the molecular bound state are not detected because they quickly decay to states that do not respond to our absorption imaging scheme.

In Fig. 1 we show on a logarithmic scale the remaining atoms as a function of time. The three datasets are recorded at 753, 832, and 1078 G with initial interaction parameters $(k_F a_s)^{-1} = 1.5, 0$ and -1.65, corresponding to the BEC, unitarity and BCS regimes, respectively. Here $k_F = (2mE_F/\hbar^2)^{1/2}$ is the Fermi momentum [25]. For better comparison, the data were normalized to the initial atomic numbers $N(t = 0)$. The laser power was adjusted so that the initial relative loss rates are the same. Further details of the measurement parameters can be found in the Supplemental Material [26]. While on the BEC side at $(k_F a_s)^{-1} = 1.5$ the loss is well described by an exponential, it is clearly nonexponential on resonance and in the BCS regime. This behavior was predicted theoretically [27] and also studied recently in [13]. The exponential decay is typical for a pure, weakly interacting, molecular ensemble which is present in the BEC limit at zero temperature. At unitarity and on the BCS side the nonexponential decays reflect the internal changes of the degenerate Fermi gas for different densities. These decays and changes go hand-in-hand with a drop of the chemical potential of the gas, see also [26].

Using Eq. (2) and the respective density-dependence of the contact in the BCS, unitarity and BEC limit one can
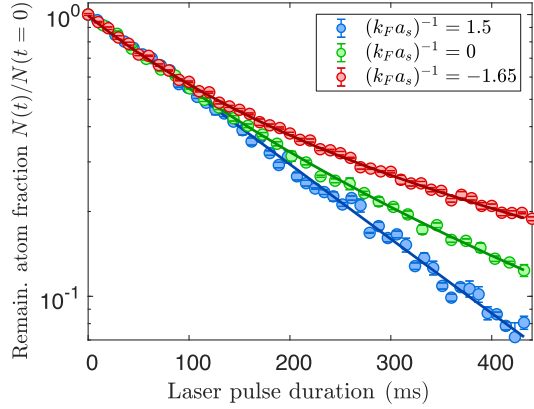
FIG. 1. Remaining atom fraction as a function of the photo-excitation laser pulse duration. The measurements were carried out at magnetic fields of 753, 832, and 1078 G with the initial $(k_F a_s)^{-1} = 1.5, 0, -1.65$ corresponding to the BEC, unitarity and BCS regimes of the crossover. The initial temperatures were $T/T_F = 0.07, 0.05,$ and 0.04, respectively. The continuous red and green lines are fits according to Eq. (3), while the blue line is an exponential (i.e. $b = \infty$).

show [22,27] that the decays at zero temperature can be described by

$$N(t) = N_0/(1 + \Gamma_0 t/b)^b \qquad (3)$$

with the initial decay rate Γ_0 and $b = 2$ in the BCS limit, $b = 6$ at unitarity and $b \to \infty$ in the BEC limit. Our fits to the data in Fig. 1 yield $b = 1.6 \pm 0.2$ at $(k_F a_s)^{-1} = -1.65$ and $b = 3.9 \pm 0.9$ at $(k_F a_s)^{-1} = 0$. For the decay curve at $(k_F a_s)^{-1} = 1.5$ we find that a pure exponential (or any $b \gtrsim 20$) fits well. Despite the quantitative deviations, this shows that we already have a qualitative understanding of the decay. The deviations might be explained by a slight increase of the atom gas temperature for long photo-excitation laser pulse durations (for further discussion see [22]). We note, however, that it is the initial loss rate Γ_0, rather than b, which is relevant for the determination of the contact $\mathcal{I}$ in our experiments. The decay rate at $t = 0$, according to Eq. (3), is simply $\dot{N} = -N_0 \Gamma_0$. At $t = 0$, the atom number is the highest and therefore uncertainties are the smallest. This has advantages compared to other methods that rely on measuring the tails of rf spectra or momentum distributions, where atomic signals are generally low. In order to get precise results we accurately determine the atom numbers, the (effective) trapping frequencies, the magnetic fields and the corresponding scattering lengths, as explained in [22] where also effects due to slight trap anharmonicities are discussed. In the following we investigate the contact in the entire BCS-BEC crossover, first for $T \approx 0$ and afterwards also for T up to $2 T_F$.

Contact in the zero temperature limit.—For $T \approx 0$ there exist already some experimental data and calculations of

the contact from other groups which we can use for comparison with our results. In our measurements we typically achieve temperatures of $T < 0.04 T_F \lesssim T_C$, where T_C is the critical temperature for superfluidity. According to Eq. (2) we need to measure dN/dt and Ω in order to determine the contact $\mathcal{I}$. We extract the initial decay rate dN/dt from decay curves which are similar to those shown in Fig. 1. Ω is given by $\Omega^2 = kI$, where I is the photo-excitation laser intensity and k is a constant which is independent of the magnetic field B and therefore of a_s. We can conveniently determine k by measuring dN/dt for a given I at an interaction regime where the contact $\mathcal{I}$ is known. [We note that when using this k, the constants γ, W and m effectively drop out of Eq. (2), see [22].] Concretely, we chose $(k_F a_s)^{-1} \gtrsim 1$ where the contact approaches the analytical result $\mathcal{I}/N k_F = 4\pi/k_F a_s$ [27]. With this calibration we can then determine $\mathcal{I}$ from measurements of dN/dt at any $(k_F a_s)^{-1}$ throughout the crossover.

Our results are shown in Fig. 2 along with theoretical calculations based on ground state energy expansions in the BCS and BEC regimes (see [22,27]). The statistical uncertainties of our data for $\mathcal{I}/N k_F$ are below 2% and the systematic errors due to anharmonic effects are below 0.3%. The solid red and dashed red lines are based on expansions up to second order (fermionic Lee-Huang-Yang correction) and up to the fourth order [28], respectively. The results apparently converge for $(k_F a_s)^{-1} < -1.5$.
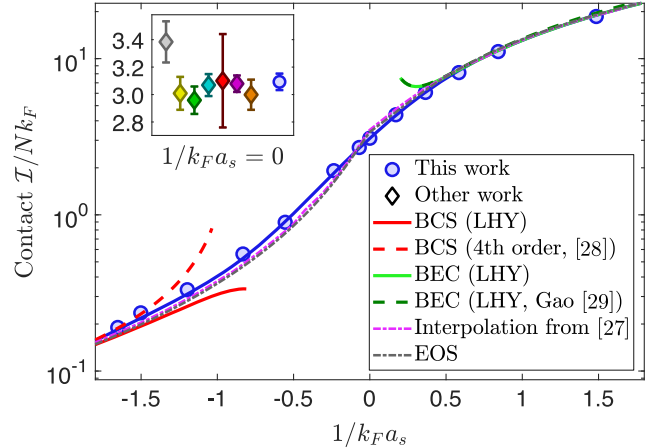
FIG. 2. Normalized contact $\mathcal{I}/N k_F$ of a harmonically trapped Fermi gas in the crossover from the BCS to the BEC regime at $T \approx 0$. Our data (blue circles) are shown together with a guide to the eye (blue line). Uncertainties are smaller or comparable to the size of the markers. Also shown are trap-integrated calculations of the contact based on different approaches (see text) as well as an interpolation [27] (purple). The inset shows our data point (blue circle) at unitarity and data from other groups (diamonds), namely, the EOS measurement [30] (gray), Bragg spectroscopy measurements by [31] (yellow) and [8] (cyan), a quantum Monte Carlo calculation [32] (green), an inelastic decay measurement [9] (red), and rf spectroscopy measurements [6] (purple) and a momentum distribution measurement [7] (orange).

The solid green and dashed dark green lines are based on the expansions to second order (bosonic Lee-Huang-Yang correction) in the BEC regime. While for the green solid line the binding energy of a dimer is calculated via $E_B = -\hbar^2/ma_s^2$, a more accurate binding energy formula is employed for the dashed dark green line [29]. This leads to a 0.6% (1.3%) larger total contact at $(k_F a_s)^{-1} = 1(2)$.

In the inset we show a comparison to other measurements and calculations at unitarity where we also find excellent agreement. In order to compare results for homogeneous systems at unitarity with values for the contact for harmonically trapped ensembles, we divided the homogeneous results by the factor $(C/nk_F^{\mathrm{hom}})/(\mathcal{I}/Nk_F) = (105\pi/256)\xi^{1/4} = 1.003$ [27], using $\xi = 0.367$ for the Bertsch Parameter [33,34]. Here, C is the homogeneous contact density, n is the atom density and k_F^{hom} is the homogeneous Fermi momentum (see also [22]). We further compare our data to calculations based on the equation of state (EOS) measurements [30] (see [22]) and an interpolation from [27]. Here, we find small deviations in the region $-1 < (k_F a_s)^{-1} < -0.2$, where we obtain slightly higher values for the contact.

The contact is closely related to the closed-channel fraction in the scattering state of two particles. In [22] we discuss this relation and compare various experimental and theoretical studies of the closed-channel fraction. The results partially differ substantially from each other.

Finite temperature contact.—We now perform measurements at various temperatures and couplings to map out the contact in the entire phase diagram of the BCS-BEC crossover. For this, we vary the temperature of our atom cloud between 0.04 and 2 T_F by changing the depth of our dipole potential for forced evaporative cooling. As a result we end up with around 5×10^4 (2×10^6) atoms at our coldest (hottest) temperatures. To tune the interaction we set the magnetic field to values between 703 G and 1080 G leading to couplings in the range $-1.5 < (k_F a_s)^{-1} < 2.5$.

Our measurement results are shown as colored circles in Fig. 3(a). Since the contact changes by 3 orders of magnitude within the investigated range of temperatures and couplings we plot the results logarithmically. By interpolating the data, we obtain a continuous map of the contact.

Close inspection shows that this map consists of slanted, parallel stripes of color. This indicates that the description of the map might be simplified within the given range. Indeed, as shown in the Supplemental Material [26], to a first approximation one can effectively replace the 2D map by a 1D function. Although this observation is interesting, at this point we cannot offer a simple physical explanation for this.

To compare our measurements to theoretical predictions we calculated the contact within the quantum virial expansion [37] as done in [38] at unitarity. These calculations are shown in Fig. 3(b) and described in detail
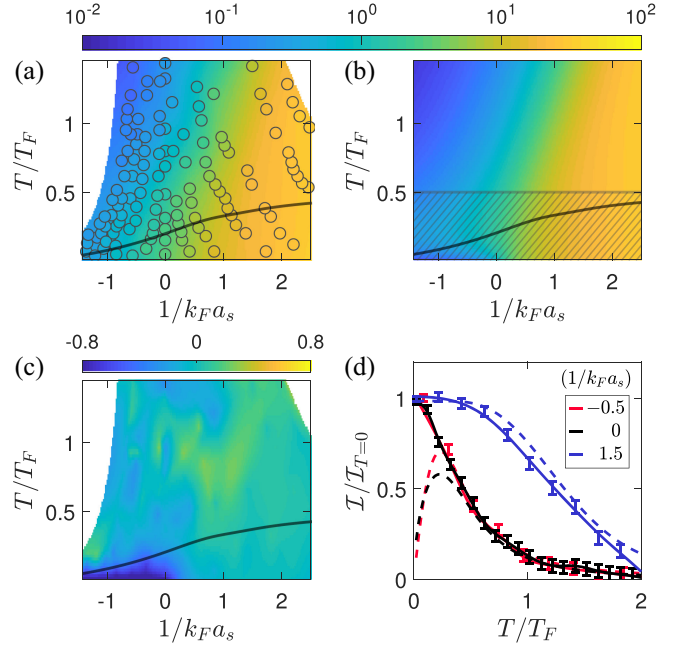
FIG. 3. Map of the contact in the BCS-BEC crossover. (a) Colored circles are measurements for the contact $\mathcal{I}/Nk_F$, where the values are indicated by the color bar. The typical statistical uncertainties are $\approx$2% (4%, 6%, 9%) for $T/T_F = 0$ (0.5, 1, 1.5) and the systematic deviations due to the trap anharmonicity are smaller than 0.3% (1.3%, 3.0%, 3.2%) for the same temperatures, see also [35]. The colored background area is an inter- and extrapolation of the measured data. The continuous black line marks the critical temperature for superfluidity T_C, taken from [36]. (b) The contact $\mathcal{I}_{QV,2}/Nk_F$ calculated from the second-order quantum virial expansion. The shaded area below $T = 0.5T_F$ marks the region where the virial expansion is expected to lose its validity. (c) Relative difference $(\mathcal{I}_{QV,2} - \mathcal{I})/\mathcal{I}$ of our measurements and the second order quantum virial calculation. (d) Contact $\mathcal{I}$ normalized by the corresponding measured zero-temperature contact as a function of temperature for three different couplings $(1/k_F a_s)^{-1}$. The data points are interpolations from the measured data in (a). The continuous lines are guides to the eye. The dashed lines are quantum virial calculations taken from (b).

in [22]. As the quantum virial expansion is a series expansion in the fugacity $z = \exp(\mu/k_B T)$, it is valid at high temperatures and low chemical potentials μ. A table of chemical potentials throughout the phase-space is provided in [26].

The calculations show that for a harmonically trapped system the virial expansion should give valid results for the contact for temperatures as low as $T = 0.5T_F$, since in this regime the fugacity is small. Below this temperature the contact values calculated with the second and third order expansion start to deviate from each other, as already discussed in [38].

Figure 3(c) is the relative difference between experimental data and the second order virial calculation. It shows that our measurements are in good agreement with the

calculations in the given range of validity at temperatures above 0.5 T_F throughout the entire crossover. On the BEC side our results agree well even down to the lowest measured temperatures of 0.04 T_F. This can be expected since the major contribution to the contact arises from the binding energy of the dimers, which is included in the second order virial expansion. At unitarity and on the BCS side for low temperatures, the Fermi gas is a system with genuine many-body correlations. Since the second-order virial expansion effectively only considers interactions between two bodies, it fails to describe these regimes quantitatively. Furthermore, on the BCS side the effective chemical potential approaches the Fermi energy at low temperatures. Therefore, the fugacity is not small anymore, violating the validity of the virial expansion. Therefore, in the low-T regime stretching from unitarity towards the BCS limit our measurements are particularly important and can serve as a benchmark for theoretical models.

The different regimes in the BCS-BEC crossover also show up very clearly in Fig. 3(d), where we plot the contact as a function of temperature for $(k_F a_s)^{-1} = -0.5$, 0, and 1.5. On the BEC side at $(k_F a_s)^{-1} = 1.5$ the dimers dominate the contribution to the contact. For low enough temperatures, when all atoms are bound in dimers, the contact is a constant (as a function of temperature). When $T \times k_B$ becomes comparable to the binding energy, the dimers become thermally unstable, break up and the contact starts decreasing [see Fig. 3(d) blue curves]. On the BCS side and at unitarity where $(k_F a_s)^{-1} \leq 0$, no weakly bound Feshbach molecular state exists. There, the decrease of the contact with increasing temperature is mainly due to overall decreasing atom density and to a breakdown of short-range pair correlations. Here, at low temperatures, our measurements for the contact strongly deviate from the results of the second-order quantum virial expansion [see Fig. 3(d) red and black curves].

Conclusion.—In conclusion, we have precisely measured Tan's contact in the full phase diagram of the BCS-BEC crossover using photoexcitation of fermion pairs. Our results bridge the gap between the well-understood BCS and BEC regimes and are in line with recent measurements and calculations at unitarity. They extend previous measurements of Tan's contact to the finite temperature regime and are consistent with the quantum virial expansion for temperatures above $0.5 T_F$.

For the future, we plan to extend our contact measurements to homogeneous Fermi gases. It has been predicted (and measured at unitarity [6]) [11,39] that a sudden change in Tan's contact should appear at the critical temperature T_C of superfluidity. Therefore, one could use such measurements to precisely map out T_C within the BCS-BEC crossover. In the harmonically trapped system this sudden change is washed out due to the inhomogeneous density distribution in the trap. In addition, we also aim for studying the contact for systems of lower dimensionality

or that feature spin imbalance. Here, probing pair correlations by measuring the contact might uncover the presence of the Fulde-Ferrell-Larkin-Ovchinnikov phase [40].

[1] S. Tan, Energetics of a strongly correlated Fermi gas, Ann. Phys. (Amsterdam) **323**, 2952 (2008).

[2] S. Tan, Large momentum part of a strongly correlated Fermi gas, Ann. Phys. (Amsterdam) **323**, 2971 (2008).

[3] S. Tan, Generalized virial theorem and pressure relation for a strongly correlated Fermi gas, Ann. Phys. (Amsterdam) **323**, 2987 (2008).

[4] J. T. Stewart, J. P. Gaebler, T. E. Drake, and D. S. Jin, Verification of universal relations in a strongly interacting Fermi gas, Phys. Rev. Lett. **104**, 235301 (2010).

[5] Y. Sagi, T. E. Drake, R. Paudel, and D. S. Jin, Measurement of the homogeneous contact of a unitary Fermi gas, Phys. Rev. Lett. **109**, 220402 (2012).

[6] B. Mukherjee, P. B. Patel, Z. Yan, R. J. Fletcher, J. Struck, and M. W. Zwierlein, Spectral response and contact of the unitary Fermi gas, Phys. Rev. Lett. **122**, 203402 (2019).

[7] C. Shkedrov, M. Menashes, G. Ness, A. Vainbaum, E. Altman, and Y. Sagi, Absence of heating in a uniform Fermi gas created by periodic driving, Phys. Rev. X **12**, 011041 (2022).

[8] S. Hoinka, M. Lingham, K. Fenech, H. Hu, C. J. Vale, J. E. Drut, and S. Gandolfi, Precise determination of the structure factor and contact in a unitary Fermi gas, Phys. Rev. Lett. **110**, 055305 (2013).

[9] S. Laurent, M. Pierce, M. Delehaye, T. Yefsah, F. Chevy, and C. Salomon, Connecting few-body inelastic decay to quantum correlations in a many-body system: A weakly coupled impurity in a resonant Fermi gas, Phys. Rev. Lett. **118**, 103403 (2017).

[10] X.-Y. Gao, D. Blume, and Y. Yan, Temperature-dependent contact of weakly interacting single-component Fermi gases and loss rate of degenerate polar molecules, Phys. Rev. Lett. **131**, 043401 (2023).

[11] J. Wang, X.-J. Liu, and H. Hu, Photoexcitation measurement of Tan's contact for a strongly interacting Fermi gas, Phys. Rev. A **104**, 063309 (2021).

[12] G. B. Partridge, K. E. Strecker, R. I. Kamar, M. W. Jack, and R. G. Hulet, Molecular probe of pairing in the BEC-BCS crossover, Phys. Rev. Lett. **95**, 020404 (2005).

[13] X.-P. Liu, X.-C. Yao, H.-Z. Chen, X.-Q. Wang, Y.-X. Wang, Y.-A. Chen, Q. Chen, K. Levin, and J.-W. Pan, Observation

of the density dependence of the closed-channel fraction of a ^{6}Li superfluid, Natl. Sci. Rev. **9,** nwab226 (2022).

[14] E. Braaten, Universal relations for fermions with large scattering length, in *The BCS-BEC Crossover and the Unitary Fermi Gas*, edited by W. Zwerger, Lecture Notes in Physics Vol. 836 (Springer, Berlin, Heidelberg, 2011), pp. 193–231, 10.1007/978-3-642-21978-8_6.

[15] E. Braaten and L. Platter, Exact relations for a strongly-interacting Fermi gas from the operator product expansion, Phys. Rev. Lett. **100,** 205301 (2008).

[16] M. He, C. Lv, H.-Q. Lin, and Q. Zhou, Universal relations for ultracold reactive molecules, Sci. Adv. **6,** 51 (2020).

[17] G. Zuern, T. Lompe, A. N. Wenz, S. Jochim, P. S. Julienne, and J. M. Hutson, Precise characterization of ^{6}Li Feshbach resonances using trap-sideband-resolved rf spectroscopy of weakly bound molecules, Phys. Rev. Lett. **110,** 135301 (2013).

[18] The measured value of $\gamma = 2\pi \times 12(1)$ MHz is in agreement with earlier measurements [19] and theoretical calculations [20] predicting a molecular linewidth of nearly twice the atomic linewidth of the $2P$ state [21].

[19] I. D. Prodan, M. Pichler, M. Junker, R. G. Hulet, and J, L. Bohn, Intensity dependence of photoassociation in a quantum degenerate atomic gas, Phys. Rev. Lett. **91,** 080402 (2003).

[20] R. Côté and A. Dalgarno, Photoassociation intensities and radiative trap loss in lithium, Phys. Rev. A **58,** 498 (1998).

[21] W. I. McAlexander, E. R. I. Abraham, and R. G. Hulet, Radiative lifetime of the $2P$ state of lithium, Phys. Rev. A **54,** R5(R) (1996).

[22] M. Jäger and J. Hecker Denschlag, companion paper, Methods for studying Tan's contact in the BCS-BEC crossover, Phys. Rev. A **109,** 063330 (2024).

[23] T. Paintner, D. K. Hoffmann, M. Jäger, W. Limmer, W. Schoch, B. Deissler, M. Pini, P. Pieri, G. C. Strinati, C. Chin, and J. Hecker Denschlag, Pair fraction in a finite-temperature Fermi gas on the BEC side of the BCS-BEC crossover, Phys. Rev. A **99,** 053617 (2019).

[24] D. K. Hoffmann, T. Paintner, W. Limmer, D. S. Petrov, and J. Hecker Denschlag, Reaction kinetics of ultracold molecule-molecule collisions, Nat. Commun. **9,** 5244 (2018).

[25] Here, we ignore the slight anharmonicity of our trap, for details see [22]. This leads to a small relative shift of k_F on the level of less than 1%.

[26] See Supplemental Material at http://link.aps.org/supplemental/10.1103/PhysRevLett.132.263401 for (i) experimental parameters for the measurements in Fig. 1, (ii) a 2D and 3D representation of our measurements, (iii) calculated central chemical potentials in our experiments, and (iv) the numerical values from our interpolation of the contact in Fig. 3(a).

[27] F. Werner, L. Tarruell, and Y. Castin, Number of closed-channel molecules in the BEC-BCS crossover, Eur. Phys. J. B **68,** 401 (2009).

[28] G. A. Baker Jr., Neutron matter model, Phys. Rev. C **60,** 054311 (1999).

[29] B. Gao, Binding energy and scattering length for diatomic systems, J. Phys. B **37,** 4273 (2004).

[30] N. Navon, S. Nascimbène, F. Chevy, and C. Salomon, The equation of state of a low-temperature Fermi gas with tunable interactions, Science **328,** 5979 (2010).

[31] E. D. Kuhnle, H. Hu, X.-J. Liu, P. Dyke, M. Mark, P. D. Drummond, P. Hannaford, and C. J. Vale, Universal behavior of pair correlations in a strongly interacting Fermi gas, Phys. Rev. Lett. **105,** 070402 (2010).

[32] J. E. Drut, T. A. Laehde, and T. Ten, Momentum distribution and contact of the unitary Fermi gas, Phys. Rev. Lett. **106,** 205302 (2011).

[33] S. Jensen, C. N. Gilbreth, and Y. Alhassid, Contact in the unitary Fermi gas across the superfluid phase transition, Phys. Rev. Lett. **125,** 043402 (2020).

[34] X. Li, X. Luo, S. Wang, K. Xie, X.-P. Liu, H. Hu, Y.-A. Chen, X.-C. Yao, and J.-W. Pan, Second sound attenuation near quantum criticality, Science **375,** 6580 (2022).

[35] The statistical uncertainties decrease with decreasing temperature T, since in our experiments evaporative cooling leads to more stable atom numbers at lower temperatures. The increase of the systematic uncertainty with T is explained in [22].

[36] D. K. Hoffmann, V. P. Singh, T. Paintner, M. Jäger, W. Limmer, L. Mathey, and J. Hecker Denschlag, Second sound in the crossover from the Bose-Einstein condensate to the Bardeen-Cooper-Schrieffer superfluid, Nat. Commun. **12,** 7074 (2021).

[37] X.-J. Liu, Virial expansion for a strongly correlated Fermi system and its application to ultracold atomic Fermi gases, Phys. Rep. **524,** 37 (2013).

[38] H. Hu, X.-J. Liu, and P. D. Drummond, Universal contact of strongly interacting fermions at finite temperatures, New J. Phys. **13,** 035007 (2011).

[39] F. Palestini, A. Perali, P. Pieri, and G. C. Strinati, Temperature and coupling dependence of the universal contact intensity for an ultracold Fermi gas, Phys. Rev. A **82,** 021605(R) (2010).

[40] U. Toniolo, B. Mulkerin, X.-J. Liu, and H. Hu, Larkin-Ovchinnikov superfluidity in a two-dimensional imbalanced atomic Fermi gas, Phys. Rev. A **95,** 013603 (2017).